AIAA JOURNAL
Vol. 35, No. 9, September 1997

Upwind Scheme for Acoustic Disturbances Generated by Low-Speed Flows

John A. Ekaterinaris*
RISOE National Laboratory, DK-4000, Roskilde, Denmark

Computation of acoustic disturbances generated by unsteady, low-speed flows, such as flows including vortices and shear layers, can be obtained by a recently proposed two-step method. This method requires a hydrodynamic field solution and obtains the acoustic field from the perturbed, inviscid, compressible flow equations. A numerical method for the solution of the equations governing the acoustic field is presented. The primitive variable form of the governing equations is used for the numerical solution. Time integration is performed with a fourth-order, Runge–Kutta method. Discretization of the primitive variables space derivatives is obtained with a high-order, upwind-biased numerical scheme. Upwinding of these convective fluxes is performed according to the eigenvalue sign of the coefficient matrices. Nonreflecting boundary conditions are applied to properly convect outgoing waves away from the computational domain. Solutions are obtained for the acoustic field generated by a pair of corotating point vortices. Computed results are compared with the existing analytic solution for the sound field.

Nomenclature

$\hat{\tilde{A}}$, $\hat{\tilde{B}}$	= flux Jacobian matrices
A, B	= coefficient matrices
c	= speed of sound
$\hat{\boldsymbol{f}}$, $\hat{\boldsymbol{g}}$	= flux vectors
P	= hydrodynamic pressure
P_0	= freestream pressure
$\bar{P}$	= average pressure
$p\prime$	= acoustic pressure
$\hat{\boldsymbol{q}}$	= vector in flow and acoustic variables
$\tilde{\boldsymbol{q}}$	= primitive variable vector
r_0	= distance between point vortices
U, V	= hydrodynamic velocity components
$u\prime$, $v\prime$	= acoustic velocity components
x, y	= Cartesian coordinates
Γ	= vortex circulation
ρ_0	= constant incompressible density
ρ_1	= density correction
$\rho\prime$	= acoustic density
ω	= angular velocity

I. Introduction

GENERATION of acoustic excitations and propagation of sound waves in low-speed, practically incompressible flowfields is a subject of theoretical interest and importance to many industrial applications. The compressible Navier–Stokes equations describe both sound generation and propagation at all flow conditions. Direct numerical simulation of the unsteady, compressible Navier–Stokes equations, when they include both the near and the far field, offers the advantage that the near-field quantities, e.g., the sources, are directly computed simultaneously with the far-field sound radiation. Direct numerical simulations for low freestream speeds, however, are prohibitively expensive for practical problems, such as blade vortex interaction in helicopter and wind turbine blades, jet noise, and other applications. Direct numerical simulations were used for simpler problems, cf. Refs. 1–3. Less computationally intensive methods, such as the numerical solution of the linearized Euler equations,[4–6] can be used for numerical predictions of sound propagation and scattering in the absence of freestream flow. These methods require a priori knowledge of the sound source and cannot be used to predict sound generation, i.e., the sound source. The idea of separating the sound sources from propagation effects was used in acoustic analogy theories, e.g., Refs. 7–9. Acoustic analogies are used for aeroacoustic predictions of low Mach number flows. The source terms in many acoustic analogies are estimated from the incompressible part of the near field.

The far-field radiation from a stationary or moving sound source with subsonic or supersonic speed can be obtained from Kirchhoff's method. This method is summarized in a recent review.[10] The Kirchhoff's method does not require a fine numerical mesh to propagate the sound to the far field and provides an advantage for far-field sound radiation predictions. It requires, however, careful selection of a smooth surface close to the sound source on which the flow variables are computed from a computational fluid dynamics (CFD) solution. Sound radiation is calculated from the computed pressure on this surface. Kirchhoff integral methods have been used with success in Refs. 11 and 12 for far-field aeroacoustic noise predictions.

Recently, Hardin and Pope[13] proposed a two-step procedure for computational aeroacoustics, which is suitable for both generation and propagation of sound in low-speed flow. This technique introduces a hydrodynamic density correction to the constant hydrodynamic density and splits the compressible Euler equations into hydrodynamic terms and perturbed acoustic terms. Computation of sound generation and propagation is carried out in two steps as follows. First, the viscous hydrodynamic flowfield is obtained either from a closed-form solution or from a numerical solution of the unsteady, incompressible flow equations. A density correction ρ_1 to the constant hydrodynamic density ρ_0 is defined through an isentropic relation. The pressure in this isentropic relation is considered to be the deviation of the instantaneous hydrodynamic pressure from its time average. The density correction relates the low-speed flowfield with the acoustic field and acts as the sound source to the compressible acoustic field. Once the density correction is defined, the acoustic radiation is obtained from the numerical solution of an inhomogeneous system of the perturbed, compressible inviscid equations, which include the density correction, the hydrodynamic flow variables, and their derivatives, in addition to the acoustic fluctuations.

The advantage of the two-step splitting approach of Hardin and Pope,[13] compared to the acoustic analogy theories is that it obtains the source strength directly from the low-speed, unsteady flow and properly accounts for sound radiation and scattering. Therefore, this approach can be used for aeroacoustic computations where the sound is generated by both compact and distributed sound sources. Sound radiation in the far field and acoustic scattering from solid bodies also can be computed.

Received Nov. 1, 1996; presented as Paper 97-0022 at the AIAA 35th Aerospace Sciences Meeting and Exhibit, Reno, NV, Jan. 6–10, 1997; revision received May 14, 1997; accepted for publication May 30, 1997.

*Senior Research Scientist, Test Station for Wind Turbines, Building AMV-762. Associate Fellow AIAA.

The technique of Ref. 13 was applied for the calculation of sound generation by a two-dimensional cavity in low-speed flow[14] and for sound radiation by a spinning vortex pair.[15] The flowfield, for both the cavity flow and the corotating vortices, is rather complex. In both cases, the sound propagates in the presence of a nonuniform flow velocity. In addition, for the cavity case, scattering from the solid walls occurs in the presence of a nonuniform flow speed. It appears, therefore, that this method can be used for aeroacoustic predictions in practical applications. The numerical solution in both Refs. 14 and 15 was obtained with the McCormack's predictor–corrector scheme. The purpose of the present paper is to apply a high-order accurate, upwind-biased numerical scheme to the solution of the equations proposed by Hardin and Pope. The same model problem of a corotating vortex pair, investigated in Ref. 15, is used to validate the numerical procedure.

The sound field from corotating vortices was investigated numerically[3] with the direct simulation of the compressible Navier–Stokes equations. It has also been the subject of theoretical works by Powell[9] and Müller and Obermeier,[16] which predicted that the generated sound is that of a rotating quadrupole. The sound field from corotating viscous vortices has not been determined analytically. For the simplified case of inviscid point vortices there is an analytic closed-form solution for both the hydrodynamic flowfield and the acoustic field. Testing of the numerical solution for this problem is facilitated because the flowfield does not need to be recomputed with different time steps and grid densities.

In the following sections, the governing equations originally given in Ref. 13 are summarized. These equations are written in a primitive variable form for the acoustic fluctuations. A space discretization procedure, suitable for the evaluation of the convective derivatives of the primitive variable form, is presented. The numerical method is tested for time and space accuracy and solutions are obtained for several flow conditions for the corotating vortices. The results are compared with the analytic solution.

II. Governing Equations

The equations governing the acoustic field induced by low-speed flows, originally presented in Ref. 13, are

$$\frac{\partial \hat{\boldsymbol{q}}}{\partial t} + \frac{\partial \hat{\boldsymbol{f}}}{\partial x} + \frac{\partial \hat{\boldsymbol{g}}}{\partial y} = \hat{\boldsymbol{h}} \tag{1}$$

where

$$\hat{\boldsymbol{q}} = \begin{pmatrix} \rho\prime \\ \rho u\prime + \rho\prime U \\ \rho v\prime + \rho\prime V \end{pmatrix}, \qquad \hat{\boldsymbol{f}} = \begin{pmatrix} \rho u\prime + \rho\prime U \\ \rho(2Uu\prime + u\prime^2) + \rho\prime U^2 + p\prime \\ \rho(Vu\prime + Uv\prime + u\prime v\prime) + \rho\prime UV \end{pmatrix}$$

$$\hat{\boldsymbol{g}} = \begin{pmatrix} \rho v\prime + \rho\prime V \\ \rho(Vu\prime + Uv\prime + u\prime v\prime) + \rho\prime UV \\ \rho(2Vv\prime + v\prime^2) + \rho\prime V^2 + p\prime \end{pmatrix}$$

$$\hat{\boldsymbol{h}} = -\begin{pmatrix} \dfrac{\partial}{\partial t}(\rho_1) + \dfrac{\partial}{\partial x}(\rho_1 U) + \dfrac{\partial}{\partial y}(\rho_1 V) \\ \dfrac{\partial}{\partial t}(\rho_1 U) + \dfrac{\partial}{\partial x}(\rho_1 U^2) + \dfrac{\partial}{\partial y}(\rho_1 UV) \\ \dfrac{\partial}{\partial t}(\rho_1 V) + \dfrac{\partial}{\partial x}(\rho_1 UV) + \dfrac{\partial}{\partial y}(\rho_1 U^2) \end{pmatrix}$$

In these equations, the acoustic fluctuations are the acoustic density $\rho\prime$ normalized by the freestream density ρ_0, the acoustic velocities $u\prime$ and $v\prime$ normalized by c_0, and the acoustic pressure $p\prime$ normalized by $\rho_0 c_0^2$. For isentropic flow, the acoustic pressure $p\prime$ is related to the instantaneous, time-dependent hydrodynamic pressure and the density $\rho = \rho_0 + \rho_1 + \rho\prime$ through the following isentropic relation $p\prime/p_0 = (\rho\prime/\rho_0)^\gamma$. The nondimensional form of the isentropic relation is

$$p\prime = (\rho^\gamma/\gamma) - P \tag{2}$$

The low-speed flowfield and the acoustic field are coupled through the variable density correction $\rho_1 = \rho_1(\boldsymbol{x}, t)$, which is defined as

$$\rho_1 = \frac{P - \bar{P}}{c_0^2}, \qquad \bar{P} = \lim_{T\to\infty} \frac{1}{T}\int_0^T P\,\mathrm{d}t \tag{3}$$

The flowfield variables U, V, and P are obtained either from the numerical solution of the time-dependent incompressible flow equations or from an analytic solution.

The equations of the acoustic field [Eqs. (1)] can be written in a form more convenient for numerical treatment as follows:

$$\hat{C}\frac{\partial \tilde{\boldsymbol{q}}}{\partial t} + \hat{A}\frac{\partial \tilde{\boldsymbol{q}}}{\partial x} + \hat{B}\frac{\partial \tilde{\boldsymbol{q}}}{\partial y} = \hat{\boldsymbol{h}} \tag{4}$$

where $\tilde{\boldsymbol{q}}$ is the primitive variable vector for the acoustic fluctuations, $\hat{A}$ and $\hat{B}$ are flux Jacobian matrices, and $\hat{C}$ is a transformation matrix:

$$\tilde{\boldsymbol{q}} = \begin{pmatrix} \rho\prime \\ u\prime \\ v\prime \end{pmatrix}, \qquad \hat{C} = \frac{\partial \hat{\boldsymbol{q}}}{\partial \tilde{\boldsymbol{q}}}, \qquad \hat{A} = \frac{\partial \hat{\boldsymbol{f}}}{\partial \tilde{\boldsymbol{q}}}, \qquad \hat{B} = \frac{\partial \hat{\boldsymbol{g}}}{\partial \tilde{\boldsymbol{q}}}$$

Multiplication of Eq. (4) with the inverse of the transformation matrix $\hat{C}^{-1}$ yields the primitive variable form of Eq. (1)

$$\frac{\partial \tilde{\boldsymbol{q}}}{\partial t} + \tilde{A}\frac{\partial \tilde{\boldsymbol{q}}}{\partial x} + \tilde{B}\frac{\partial \tilde{\boldsymbol{q}}}{\partial y} = \tilde{\boldsymbol{s}} \tag{5}$$

where $\tilde{A}$ and $\tilde{B}$ are coefficient matrices and $\tilde{\boldsymbol{s}}$ is the source term in primitive variables. These terms are obtained by

$$\tilde{A} = \hat{C}^{-1}\hat{A}, \qquad \tilde{B} = \hat{C}^{-1}\hat{B}, \qquad \tilde{\boldsymbol{s}} = \hat{C}^{-1}\hat{\boldsymbol{h}}$$

The coefficient matrices and the source term for a Cartesian coordinates system are given in the Appendix. The form of these matrices is given for both isentropic flow, where the acoustic pressure is obtained from Eq. (3), and for general flow, where the acoustic pressure is obtained from a homogeneous equation for acoustic pressure as suggested in Ref. 13. Equation (5) is the primitive variable form of Eq. (1) and is used for the numerical solution along with the appropriate boundary conditions at the far-field boundaries of the computational domain.

III. Boundary Conditions

Boundary conditions for aeroacoustic computations were tested in Ref. 6. It was found that the Tam and Webb[4] boundary condition, which is also the simplest to implement, performs better than other nonreflecting boundary conditions in use to aeroacoustics. Therefore, at the far field of the computational domain, the Tam and Webb[4] acoustic radiation boundary condition is applied and the acoustic variables are obtained from

$$\left[\frac{1}{(V_r + c)}\frac{\partial}{\partial t} + \cos\theta\frac{\partial}{\partial x} + \sin\theta\frac{\partial}{\partial y} + \frac{1}{2r}\right]\boldsymbol{q}_b = 0 \tag{6}$$

The vector $\boldsymbol{q}_b$ contains the far-field variables $\boldsymbol{q}_b = [\rho\prime + \rho_1, u\prime, v\prime]^T$ at the boundaries, $V_r = (U + u\prime)\cos\theta + (V + v\prime)\sin\theta$, and $r = \sqrt{(x^2 + y^2)}$ and θ are the polar distance and angle between the boundary point and the source. It was shown in Ref. 4 that the accuracy of this boundary condition is of order $r^{-5/2}$ and the accuracy increases exponentially with the distance r of the boundary point from the source. The time derivative in Eq. (6) is discretized with a first-order accurate formula and the variables $\boldsymbol{q}_b$ at the computational boundaries are updated explicitly.

IV. Numerical Implementation

The perturbed Euler equations given in the preceding section [Eqs. (1)] have been solved numerically in Refs. 14 and 15 using the explicit, predictor–corrector, MacCormack scheme, which is second-order accurate in both space and time. In this paper the primitive variable form of the governing equations [Eqs. (5)] is used. Time integration of the primitive variable form of the governing equations can be obtained either with explicit or implicit methods. In any case, time accuracy is required for the inherently unsteady aeroacoustic

problems, and a scheme with sufficient time accuracy[4,17] must be used. An explicit time-integration scheme is chosen because it is less computationally intensive compared to implicit schemes and can provide high order of accuracy.

A. Time Marching

The Hardin and Pope splitting method allows the separation of the computation of the viscous hydrodynamic field and the acoustic field. The flow computation requires a highly stretched viscous mesh in the regions of large flow gradients. The acoustic field computation does not require a highly stretched mesh similar to the one used for the hydrodynamic computation. As a result, the numerical stability limitations for the acoustic field computation are not as severe as for the viscous flowfield computation, and an explicit scheme may be used for time integration of the equations governing the acoustics. Large time steps in time marching and a high order of time accuracy can be obtained with the following low-storage, fourth-order Runge–Kutta method:

$$q^0 = q^n, \qquad q^1 = q^0 + c_1 R(q^0), \qquad q^2 = q^0 + c_2 R(q^1)$$
$$q^3 = q^0 + c_3 R(q^2), \qquad q^4 = q^0 + c_4 R(q^3), \qquad q^{n+1} = q^4 \tag{7}$$

where q^n is the primitive variable vector at time level n, R is the right-hand-side residual term, and c_i are the Runge–Kutta coefficients. In Ref. 17, higher-order methods for time integration in aeroacoustic computations were tested. It was found that higher-order time accuracy does not yield improvements compared to the classical fourth-order method.

B. Space Discretization

The matrices $\tilde{A}$ and $\tilde{B}$ are diagonalized as follows:

$$A\pm = X_A \Lambda\pm_A X_A^{-1}, \qquad B\pm = X_B \Lambda\pm_B X_B^{-1} \tag{8}$$

where Λ_A and Λ_B are diagonal matrices containing the eigenvalues of $\tilde{A}$ and $\tilde{B}$, X_A and X_B are the left eigenvector, and X_A^{-1} and X_B^{-1} are the right eigenvector matrices of $\tilde{A}$ and $\tilde{B}$, respectively. These matrices are given in the Appendix. After diagonalization, $\tilde{A} = A^+ + A^-$ and $\tilde{B} = B^+ + B^-$, where A^+ and A^- contain only positive and only negative eigenvalues, respectively.

The convective terms $\tilde{q}_x = \partial\tilde{q}/\partial x$, $\tilde{q}_y = \partial\tilde{q}/\partial y$ are computed using upwind differences based on the sign of eigenvalues of the coefficient matrices $\tilde{A}$ and $\tilde{B}$. This method was originally proposed by Courant et al.[18] as a finite difference scheme for the solution of hyperbolic equations, and it was used[19] for the solution of the compressible Euler equations. The right-hand-side residual term R, of Eqs. (7), $\partial\tilde{q}/\partial t = R = \tilde{s} - (\tilde{A}\tilde{q}_x + \tilde{B}\tilde{q}_y)$, is computed as

$$R = \tilde{s} - \left[(A^+\tilde{q}_x^- + A^-\tilde{q}_x^+) + (B^+\tilde{q}_y^- + B^-\tilde{q}_y^+) \right] \tag{9}$$

where q^- and q^+ are evaluated with backward and forward upwind difference operators, respectively. First-order upwinding is too diffusive to produce a solution with reasonable number of grid points. Therefore, higher-order, upwind-biased formulas are used to evaluate the derivatives $\tilde{q}_x = \partial\tilde{q}/\partial x$ and $\tilde{q}_y = \partial\tilde{q}/\partial y$ as follows.

Third-order accuracy is obtained for

$$\tilde{q}_x^+ = \tfrac{1}{6}(-\tilde{q}_{i+2} + 6\tilde{q}_{i+1} - 3\tilde{q}_i - 2\tilde{q}_{i-1})$$
$$\tilde{q}_x^- = \tfrac{1}{6}(2\tilde{q}_{i+1} + 3\tilde{q}_i - 6\tilde{q}_{i-1} + \tilde{q}_{i-2}) \tag{10}$$

fourth-order accuracy for

$$\tilde{q}_x^+ = \tfrac{1}{12}(\tilde{q}_{i+3} - 6\tilde{q}_{i+2} + 18\tilde{q}_{i+1} - 10\tilde{q}_i - 3\tilde{q}_{i-1})$$
$$\tilde{q}_x^- = \tfrac{1}{12}(3\tilde{q}_{i+1} + 10\tilde{q}_i - 18\tilde{q}_{i-1} + 6\tilde{q}_{i-2} - \tilde{q}_{i-3}) \tag{11}$$

and fifth-order accuracy for

$$\tilde{q}_x^+ = \tfrac{1}{60}(+2\tilde{q}_{i+3} - 15\tilde{q}_{i+2} + 60\tilde{q}_{i+1} - 20\tilde{q}_i - 30\tilde{q}_{i-1} + 3\tilde{q}_{i-2})$$
$$\tilde{q}_x^- = \tfrac{1}{60}(-3\tilde{q}_{i+2} + 30\tilde{q}_{i+1} + 20\tilde{q}_i - 60\tilde{q}_{i-1} + 15\tilde{q}_{i-2} - 2\tilde{q}_{i-3}) \tag{12}$$

Most of the computing time at each time step is spend to construct the $A\pm$ and $B\pm$ matrices. Once these matrices are constructed, a higher order of accuracy can be obtained for a very small additional computing cost using Eqs. (11) or (12) instead of Eqs. (10). The proposed method based on the primitive variable formulation of the governing equations provides a higher order of accuracy in both space and time compared to the second-order accurate methods used in Refs. 14 and 15. A higher order of accuracy is important for aeroacoustic computations[4,6,17] because it reduces dispersion errors.

V. Results and Discussion

The two-step splitting technique for computational aeroacoustics proposed by Hardin and Pope[13] appears to be a practical approach for the prediction of sound fields generated by low-speed practically incompressible flows. Predictions obtained for sound generation, propagation and scattering from low-speed flow over a cavity[14] have shown good agreement with the experiment. Computation of a similar sound field, however, has as a prerequisite the accurate computation of the unsteady flowfield so that a time-average pressure is obtained from the time periodic solution and perturbation of the hydrodynamic density can be defined. As a result, testing of numerical methods for the equations governing the acoustic part of the problem alone becomes time consuming for problems where the flowfield cannot be obtained from an analytic solution.

Recently, Lee and Koo[15] applied Hardin and Pope's[13] technique to the computation of sound generation from a corotating vortex pair. For this problem, there is an analytic, closed-form solution for the flowfield. Therefore, testing of the present numerical scheme proposed for the solution of the equations governing the acoustics is performed for this problem because time and space resolution studies are performed efficiently and without ambiguity. Computed results obtained with different grid densities, time steps, and order of accuracy for the evaluation of the convective terms are compared with the closed-form solution. The acoustic field solution for the corotating vortex pair was obtained in Ref. 16 with the method of matched asymptotic expansions (MAE).

A. Analytical Solution

The corotating vortex pair consists of two point vortices, which are separated by a fixed distance and rotate around each other with period $T = 8\pi^2 r_0^2/\Gamma$, where r_0 is the half-distance between the vortex centers and Γ is the vortex circulation. The corotating vortices and a sample numerical mesh used for the calculations is shown in Fig. 1. The inherent unsteadiness of the corotating vortex flowfield generates sound. Each vortex induces on the other a velocity $v_\theta = \Gamma/4\pi r_0$. A rotating Mach number is defined from v_θ as $M_r = v_\theta/c_0 = \Gamma/(4\pi r_0 c_0) = 2\pi/T$, where c_0 is the freestream speed of sound. It was shown in Ref. 20 that the quadrupole characteristics are a function of M_r and that for $M_r \leq 0.1$ the corotating vortices are acoustically compact. The flowfield is obtained from a complex potential function. The flow velocities, the hydrodynamic pressure, and the acoustic pressure fluctuation are given by

$$U - iV = \frac{\Gamma}{i\pi}\frac{z}{z^2 - b^2}$$

$$P = P_0 + \rho_0 \frac{\Gamma\omega}{\pi}\left[\Re\left(\frac{b^2}{z^2 - b^2} \right) - \frac{\Gamma r}{2\pi\omega R} \right]$$

$$P_{av} = P_0 - \rho_0 \frac{\Gamma^2}{2\pi^2}\frac{r^2}{r^4 - r_0^4}$$

$$p' = p'_A [J_2(kr)\cos(\Phi) - Y_2(kr)\sin(\Phi)]$$

$$p'_A = \frac{\rho_0 \Gamma^4}{64\pi^3 r_0^4 c_0^2}, \qquad \Phi = 2(\omega t - \theta)$$

where $z = x + iy = re^{i\theta}$, $b = r_0 e^{i\omega t}$, $\Re$ denotes the real part of a complex quantity, $\omega = \Gamma/4\pi r_0^2$ is the angular speed, $R = \sqrt{(z^2 - b^2)}$, $k = 2\omega/c_0$, and $J_2(z)$ and $Y_2(z)$ are the second-order Bessel functions of the first and second kind, respectively. The vortex sound theory proposed by Möhring[21] was also used to predict sound from acoustically compact vortical flows. Application of this theory[3] yielded a quadrupole expression for the acoustic pressure equivalent to the one derived in Ref. 16 with the MAE solution.

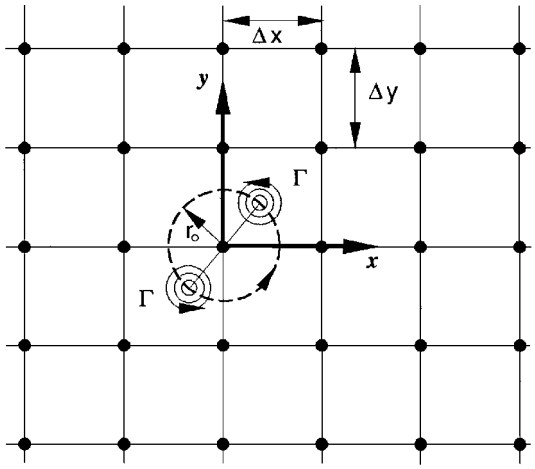

Fig. 1 Corotating vortices and mesh used for the numerical solution.

The strength of the vortices is proportional to the circulation Γ, which also determines M_r and the intensity and frequency of the acoustic field. At middle distance between the point vortices, which is the coordinate system origin, the acoustic pressure $p\prime$ becomes singular and very close to the vortex centers the hydrodynamic velocities and pressure have large gradients. In Ref. 15 a vortex core model was used to replace the point vortices. The vortex core model is not used, instead the mesh points are placed far enough from the vortex centers. For grid points located closer than the point vortex separation distance r_0 convergence cannot be obtained.

A Cartesian grid is used for the numerical solution. The computational domain is centered at the origin, which is also the location of the source, and contains the same number of grid points from the origin to far-field boundaries. The minimum grid spacing, $\Delta x = \Delta y$, for which a smooth solution without a vortex core model can be obtained, is $\Delta x \geq 2.1 r_0$, where $r_0 = 1$ because it is used as reference length. Solutions are computed for $M_r = 0.05$, $\Gamma = 2\pi/10$, and $M_r = 0.075$ and 0.10. The first case is an example of a representative low-frequency sound field, and the higher rotation Mach numbers are examples of faster rotation and higher frequency cases. Grid spacing of $\Delta x = 2.2$ provides approximately 20 points per wavelength for the highest frequency case ($M_r = 0.10$) considered in this study.

The acoustic field computation starts from zero values of acoustic density and velocity fluctuations. Acoustic waves are generated initially at the source, where the flow gradients are the largest. As the unsteady computation progresses, these waves propagate from the origin outward to the computational boundaries at a rate approximately one wavelength per cycle. The solution reaches time periodicity, when the waves formed at startup are convected outside of the domain. Depending on the size of the computational domain, approximately four to five cycles are required to achieve time periodic response. The acoustic field generated at $M_r = 0.05$ is chosen as the representative case for which numerical accuracy tests are conducted. Time and space resolution studies are performed, and the accuracy of the numerical solution is demonstrated by detailed comparisons with the analytic solution. The space and time resolution requirements for the numerical solution are identified. Improvements obtained by using a higher order of accuracy for the derivative evaluation are shown. Finally, results for higher frequency cases are presented.

B. Solution for $M_r = 0.05$

The size of the computational domain is determined by the order of accuracy provided by the boundary condition ($r^{-5/2}$) and the level of the acoustic variables at the boundary. The magnitude of acoustic pressure is proportional to the vortex circulation or the rotational Mach number M_r. For low rotational Mach number or vortex circulation, the acoustic pressure level is small. Therefore, in the computations, the lower the circulation or M_r is, the larger the required extent of the computational domain becomes. In general, domains that include three to four wavelengths in each direction were found sufficiently large for accurate solutions. Computations

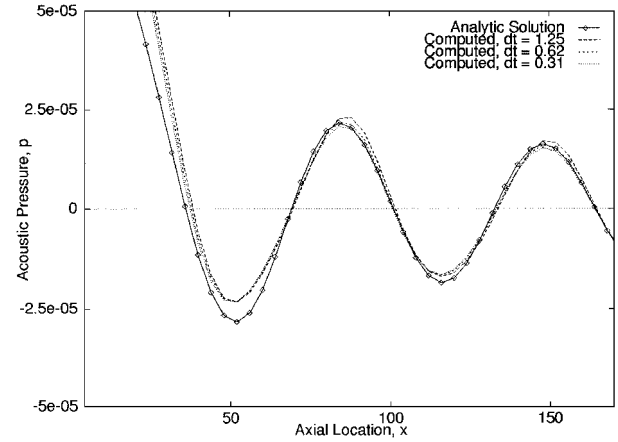

Fig. 2 Effect of computational time step on space resolution for solutions computed with $\Delta t_1 = 1.25$ ($N_T = 100$), $\Delta t_2 = 0.50\Delta t_1$, and $\Delta t_3 = 0.25\Delta t_1$; $M_r = 0.10$ and $\Gamma = 2\pi/10$.

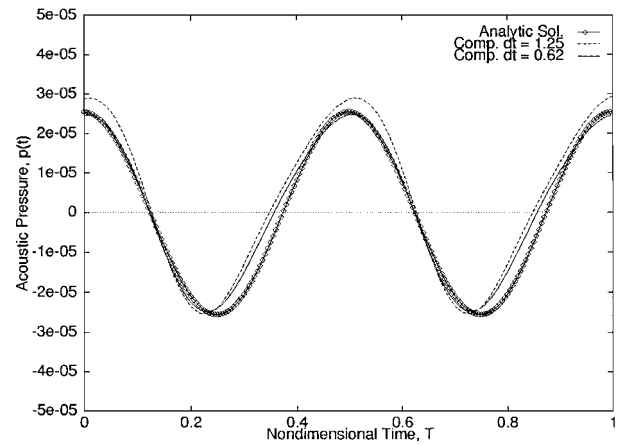

Fig. 3 Effect of computational time step on time resolution for solutions computed with $\Delta t_1 = 1.25$ ($N_T = 100$) and $\Delta t_3 = 0.25\Delta t_1$; $M_r = 0.10$ and $\Gamma = 2\pi/10$.

in larger domains, which included approximately six wavelengths in each direction, have been obtained. The computed solution did not show any difference compared to the solution computed in the smaller domain.

The effect of the time step is investigated first. The same domain with grid spacing $\Delta x = 4.0$ is used. Solutions are computed with 100, 200, and 400 time steps per cycle or $\Delta t = 1.225$, 0.62, and 0.31, respectively. The numerical solution does not converge for time steps $\Delta t \geq 2$, which appears to be the stability limit for time integration. A comparison of the computed acoustic pressures along the horizontal direction at the same time after convergence is shown in Fig. 2. The points on the analytic solution mark the location where the numerical grid points are located. All of the numerical solutions do not follow as closely the rapid variations of pressure predicted by the theory approximately half-wavelength from the source. The computations match the theoretical predictions approximately half-wavelength away from the source. The solution computed with the largest time step shows the maximum deviation from the analytic results. A comparison of the computed acoustic pressure variation over one time period at a point located 2.5 wavelengths away from the source, with the analytic solution, is shown in Fig. 3. The solutions computed with $\Delta t = 0.62$ and 0.31 are identical, whereas the solution computed with $\Delta t = 1.25$ shows larger phase errors compared with the solution that is computed with a smaller time step. Therefore, all of the other solutions are computed for time steps of $\Delta t \approx 0.5$. The overall qualitative agreement of the computed acoustic pressure with the analytic solution is shown in Fig. 4, where the pressure levels along the diagonal direction are compared. The overall agreement of numerical solution with the analytic solution is excellent. Even at the region close to the origin the numerical solution has rather small relative error with respect to the analytic predictions.

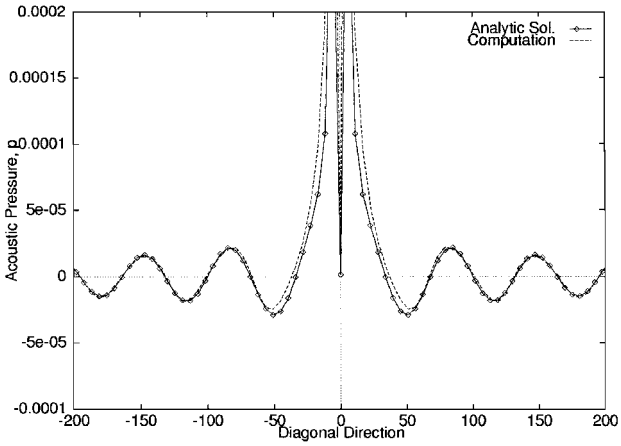

Fig. 4 Comparison of computed and analytic solutions along a diagonal direction; $\Delta t = 0.62$; $M_r = 0.10$ and $\Gamma = 2\pi/10$.

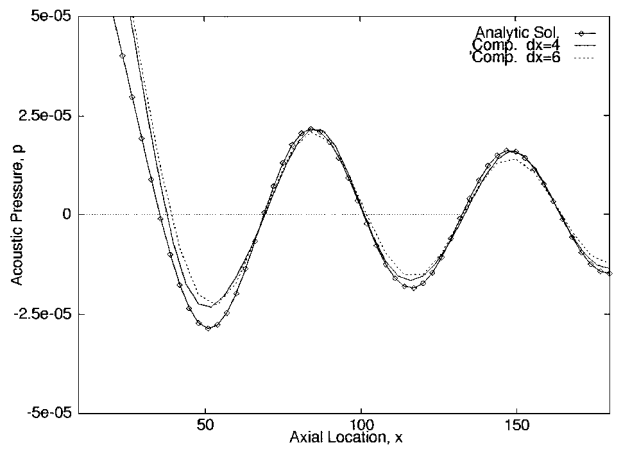

Fig. 5 Effect of grid spacing on space resolution, for solutions computed with $\Delta x_1 = 4.0$ and $\Delta x_2 = 6.0$; $M_r = 0.10$ and $\Gamma = 2\pi/10$.

A grid resolution study is performed next and computed solutions for $M_r = 0.05$, in domains of the same extent and with grid spacings of $\Delta x = 3$, 4, and 6 nondimensional units, are compared with the analytic solution. The same time step $\Delta t = 0.62$ is used for these computations. Figure 5 shows a comparison of the computed acoustic pressure along the horizontal axis with the analytic solution. The solutions computed with $\Delta x = 3$ and 4 are practically identical. The solutions computed with $\Delta x = 6$, which provides less than 20 points per wavelength, shows deviations from the analytic solution and the results computed with a higher grid density. It appears, therefore, that a minimum of 20 points per wavelength is required for the numerical solution. The acoustic pressure variation over one time period for a point located at $R = 2.5\lambda$ away from the source, obtained from the solutions computed with two different grid spacings, is compared in Fig. 6 with the analytic solution. It is seen that poor grid resolution causes larger phase errors.

The effect of the order of accuracy used to evaluate the convective terms is shown next. Two solutions computed with $\Delta t = 0.62$ or 200 time steps per cycle, $\Delta x = 4$, and using third- and fifth-order-accurate upwind formulas, respectively, are compared in Fig. 7. A solution computed with $\Delta x = 6$ and fifth order of accuracy is also shown. The solution computed with fifth order of accuracy and $\Delta x = 4$, is practically indistinguishable from the analytic solution away from the source. Increased order of accuracy improves the solution quality. Also, the solution computed with $\Delta x = 6$ and higher order of accuracy shows the same agreement with the analytic predictions as the solution computed with lower order of accuracy and more grid points per wavelength. The relative error of each solution with respect to the analytic solution over one time period is shown in Fig. 8. The fifth-order-accurate computation is indistinguishable from the analytic solution away from the origin. Higher order of accuracy also reduces the phase errors. A negligible increase of CPU

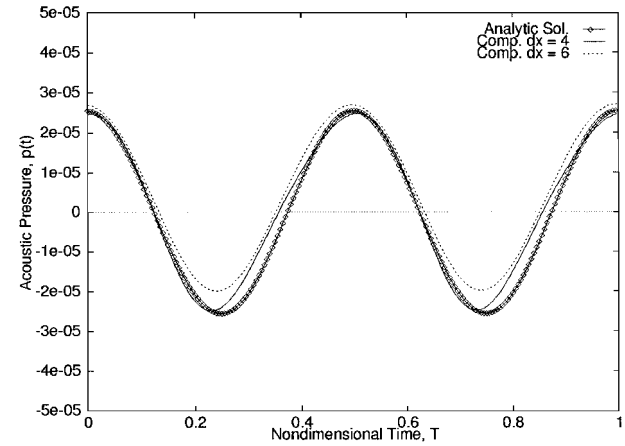

Fig. 6 Effect of grid spacing on time resolution, for solutions computed with $\Delta x_1 = 4.0$ and $\Delta x_2 = 6.0$; $M_r = 0.10$ and $\Gamma = 2\pi/10$.

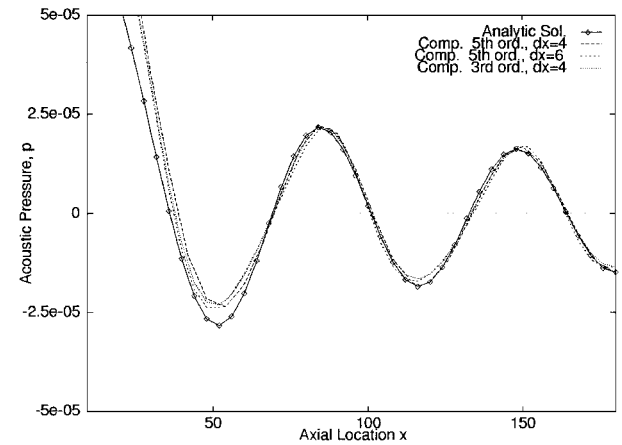

Fig. 7 Effect of the order of accuracy on space resolution for solutions computed with third- and fifth-order formulas; $M_r = 0.10$ and $\Gamma = 2\pi/10$.

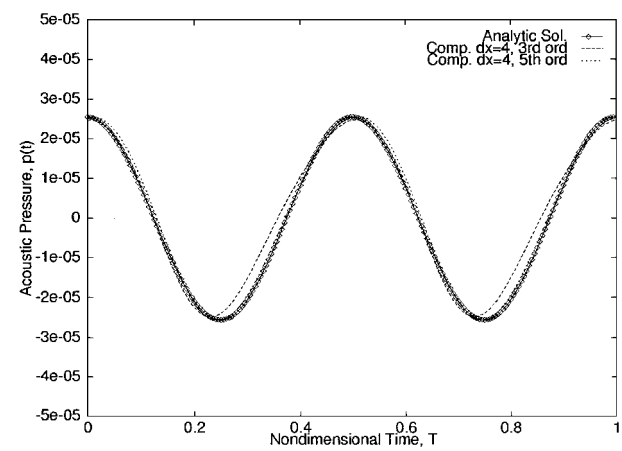

Fig. 8 Effect of the order of accuracy on time resolution for solutions computed with third- and fifth-order formulas; $M_r = 0.10$ and $\Gamma = 2\pi/10$.

time, approximately 2% more than the baseline third-order-accurate solution, is only required to obtain the fifth-order-accurate solution.

The pressure contour plot of Fig. 9 shows the overall qualitative agreement of the computed solution with the analytic predictions. The numerical solution predicts well the two-dimensional wave pattern, which becomes almost cylindrical in the far field. It appears, therefore, that the one-dimensional upwind character of the space discretization scheme still enables capturing of two-dimensional waves with a numerical mesh that is not aligned with the wave fronts. Solutions for two higher rotational Mach numbers, $M_r = 0.075$ and 0.1, are presented next.

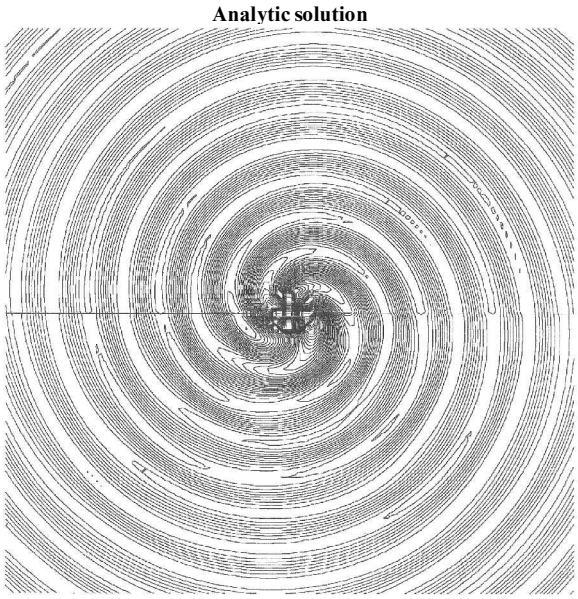

Fig. 9 Comparison of the computed acoustic pressure field with the analytic solution; $M_r = 0.10$ and $\Gamma = 2\pi/10$.

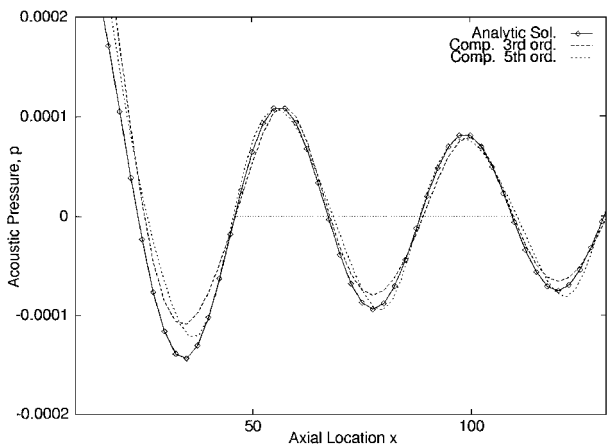

Fig. 10 Comparison of the computed acoustic pressure along the x axis with the analytic solution; $M_r = 0.075$ and $\Gamma = 3\pi/10$.

C. Solution for $M_r = 0.075$

A solution of the corotating vortex pair sound field for $M_r = 0.075$ is obtained. For this case the frequency is higher and a grid spacing of $\Delta x = 3.0$ is used in order to obtain sufficient number of grid points per wavelength. A domain that contains approximately four wavelengths in every direction is used for numerical solution and the time step is fixed to $\Delta t = 0.62$. The acoustic pressure along the axial direction obtained using the third- and fifth-order schemes is compared with the analytic solution, as shown in Fig. 10. The agreement is good, and improved resolution is obtained with the higher-order method. The time accuracy of both solutions is shown in Fig. 11, where the acoustic pressure variation over a period is compared. The qualitative agreement of the computed solution with the analytic results is shown in the pressure contour plot of Fig. 12.

D. Solution for $M_r = 0.10$

A solution of the corotating vortex pair sound field for $M_r = 0.10$ is obtained. For this case, the frequency is higher and a grid spacing of $\Delta x = 2.2$ is used to provide sufficient number of grid points per wavelength. A domain that contains approximately four wavelengths in every direction is used for the numerical solution, and the time step is fixed to $\Delta t = 0.62$. The acoustic pressure along the positive x axis obtained from solutions computed using the third- and fifth-order schemes is compared with the analytic solution, as shown in Fig. 13. Improved resolution is obtained when a higher order of

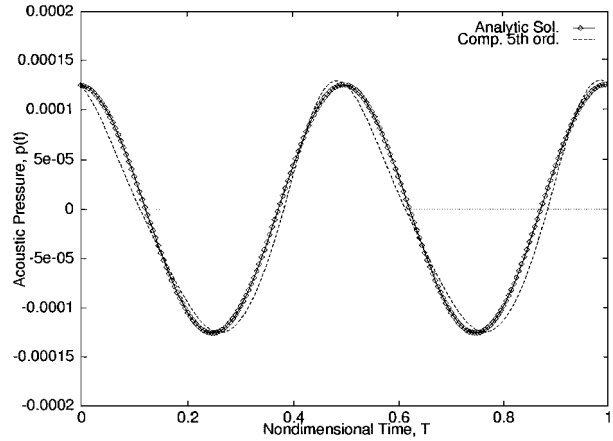

Fig. 11 Comparison of the computed acoustic pressure over one period with the analytic solution; $M_r = 0.075$ and $\Gamma = 3\pi/10$.

Fig. 12 Comparison of the computed acoustic pressure field with the analytic solution; $M_r = 0.075$ and $\Gamma = 3\pi/10$.

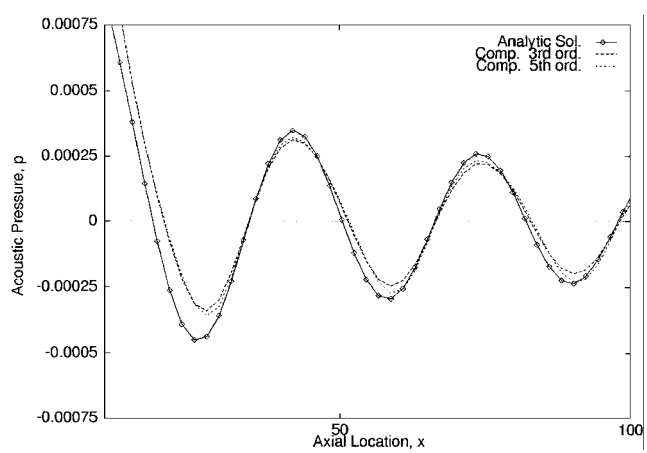

Fig. 13 Comparison of the computed acoustic pressure along the x axis with the analytic solution; $M_r = 0.10$ and $\Gamma = 4\pi/10$.

accuracy is used. Even though the grid spacing is decreased, this solution shows larger deviation from the analytic results compared to the lower-frequency cases of Figs. 7 and 8. The time accuracy of both solutions is shown in Fig. 14, where the acoustic pressure variation over a period is compared. The qualitative agreement of the computed solution with the analytic results is shown in the acoustic pressure contour plot of Fig. 15. The computations were performed on a single processor of a power challenge SGI machine, where they

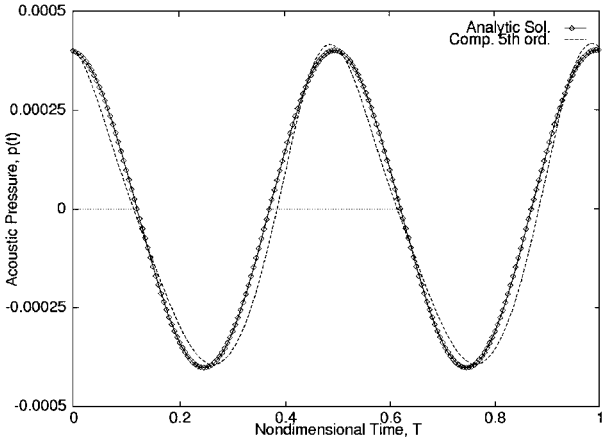

Fig. 14 Comparison of the computed acoustic pressure over one period with the analytic solution; $M_r = 0.10$ and $\Gamma = 4\pi/10$.

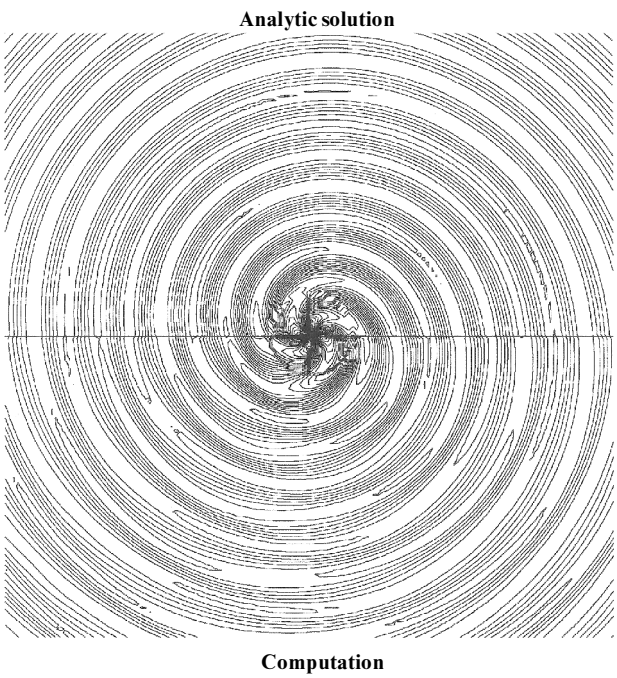

Fig. 15 Comparison of the computed acoustic pressure field with the analytic solution; $M_r = 0.10$ and $\Gamma = 4\pi/10$.

required 1.325×10^{-5} CPU s per time step per grid point. A typical computation requires 15–20 min of CPU time.

Computation of higher-frequency sound fields is, in principle, possible. However, for the corotating vortices, computations of higher-frequency fields, corresponding to higher rotation Mach numbers, would allow very few points per wavelength. The solutions of Figs. 11 and 14, which are computed with the same grid, show that the agreement of the computation with the analytic solution deteriorated for the higher-frequency case where fewer point per wavelength are used. Grid spacing limitations, imposed by the singular nature of the field at the origin, can be overcome by using curvilinear stretched meshes or a vortex core model, as in Ref. 15. Besides this limitation, the sound field generated by the corotating vortex pair is a good test problem for the evaluation of numerical methods in aeroacoustics. The numerical solution is in good agreement with the analytic solutions. Results obtained from the solution of the three-equation system, where the acoustic pressure is obtained from the isentropic relation, or the four-equation system, where the pressure is obtained as part of the solution, did not show any difference. The numerical method has good wave-capturing capabilities and produces solutions with sufficient space accuracy and small phase errors. It appears that the present numerical scheme can be applied to more complex problems. Application of the method to curvilinear meshes is straightforward.

VI. Conclusions

An upwind-biased numerical method for the solution of the equations governing generation and propagation of aeroacoustic disturbances caused by unsteady low-speed flows is presented. This scheme is applied to the primitive variable form of the governing equations. It performs time integration with a fourth-order Runge–Kutta method and for space discretization uses upwind-biased formulas based on the eigenvalue sign of the coefficient matrices. The numerical method is tested for the acoustic field generated by a corotating vortex pair. The numerical solution is in good agreement with the analytic solution. The method has good time and space resolution. A higher order of accuracy for the evaluation of the convective fluxes improves the solution at a very small computational cost. Application of the numerical scheme to curvilinear meshes is straightforward, and extension to three dimensions is possible.

Appendix: Eigenvalue and Eigenvector Matrices

The primitive variable vector form of equations governing the acoustic field is

$$\frac{\partial \rho'}{\partial t} + \boldsymbol{v}\cdot\nabla\rho' + \rho\nabla\cdot\boldsymbol{v}' = -\left[\frac{\partial \rho_1}{\partial t} + \boldsymbol{v}\cdot\nabla\rho_1\right]$$

$$\frac{\partial \boldsymbol{v}'}{\partial t} + \boldsymbol{v}\cdot\nabla\boldsymbol{v}' + \frac{\nabla p'}{\rho} = -\left[\bar{\rho}\frac{\partial \boldsymbol{V}}{\partial t} + (\bar{\rho}\boldsymbol{V} + \boldsymbol{v}')\cdot\nabla\boldsymbol{V}\right]$$

$$\frac{\partial p'}{\partial t} + \boldsymbol{v}\cdot\nabla p' + \rho c^2\nabla\cdot\boldsymbol{v}' = 0$$

where $\boldsymbol{v} = \boldsymbol{V} + \boldsymbol{v}'$, and $\boldsymbol{V}$ is the flow velocity vector, $\boldsymbol{v}'$ is the acoustic velocity vector, $\rho = \rho_0 + \rho_1 + \rho'$, and $\bar{\rho} = (\rho_1 + \rho')/\rho$. The last equation (see Ref. 13) gives the pressure variation in a general flow. For isentropic flow the pressure is obtained from the algebraic equation (2). The source term $\tilde{\boldsymbol{s}}$ is given by

$$\tilde{\boldsymbol{s}} = \begin{bmatrix} \dfrac{\partial \rho_1}{\partial t} + u\dfrac{\partial \rho_1}{\partial x} + v\dfrac{\partial \rho_1}{\partial y} \\ \bar{\rho}\dfrac{\partial U}{\partial t} + (\bar{\rho}U + u')\dfrac{\partial U}{\partial x} + (\bar{\rho}V + v')\dfrac{\partial U}{\partial y} \\ \bar{\rho}\dfrac{\partial V}{\partial t} + (\bar{\rho}U + u')\dfrac{\partial V}{\partial x} + (\bar{\rho}V + v')\dfrac{\partial V}{\partial y} \\ 0 \end{bmatrix}$$

The matrices $\tilde{A}$, $\tilde{B}$, $\Lambda_{\tilde{A}}^{\pm}$, $\Lambda_{\tilde{B}}^{\pm}$, X_A, and X_A^{-1} for the three-equation system valid isentropic flow are

$$[\tilde{A}] = \begin{bmatrix} u & \rho & 0 \\ c^2/\rho & u & 0 \\ 0 & 0 & u \end{bmatrix}, \qquad [\tilde{B}] = \begin{bmatrix} v & 0 & \rho \\ 0 & v & 0 \\ c^2/\rho & 0 & v \end{bmatrix}$$

where $u = U + u'$, c is the local speed of sound,

$$c^2 = \frac{\partial p'}{\partial \rho} = (\rho_0 + \rho_1 + \rho')^{(\gamma-1)} = \frac{\gamma(P + p')}{\rho}$$

and

$$\Lambda_{\tilde{A}}^{\pm} = \mathrm{diag}[u, u \mp c, u + c], \qquad \Lambda_{\tilde{B}}^{\pm} = \mathrm{diag}[v, v \mp c, v + c]$$

$$[X_A] = \begin{bmatrix} 0 & -\rho/c & \rho/c \\ 0 & 1 & 1 \\ 1 & 0 & 0 \end{bmatrix}, \qquad [X_A]^{-1} = \begin{bmatrix} 0 & 0 & 1 \\ -c/2\rho & 1/2 & 0 \\ c/2\rho & 1/2 & 0 \end{bmatrix}$$

and similarly for $[X_B]$ and $[X_B]^{-1}$.

The matrices A, B, $\Lambda_A^{\pm}$, $\Lambda_B^{\pm}$, X_A, and X_A^{-1} for the four-equation system describing a general flow situation are

$$[\tilde{A}] = \begin{bmatrix} u & \rho & 0 & 0 \\ 0 & u & 0 & 1/\rho \\ 0 & 0 & u & 0 \\ 0 & \rho c^2 & 0 & u \end{bmatrix}, \qquad [\tilde{B}] = \begin{bmatrix} v & 0 & \rho & 0 \\ 0 & v & 0 & 0 \\ 0 & 0 & v & 1/\rho \\ 0 & 0 & \rho c^2 & v \end{bmatrix}$$

$$\Lambda_{\tilde{A}}^{\pm} = \mathrm{diag}[u, u, u \mp c, u + c], \qquad \Lambda_{\tilde{B}}^{\pm} = \mathrm{diag}[v, v, v \mp c, v + c]$$

$$[X_A] = \begin{bmatrix} 0 & 1 & 1/c^2 & 1/c^2 \\ 0 & 1 & -1/(\rho c) & 1/(\rho c) \\ 1 & 0 & 0 & 0 \\ 0 & 0 & 1 & 1 \end{bmatrix}$$

$$[X_A]^{-1} = \begin{bmatrix} 0 & 0 & 1 & 0 \\ 1 & 0 & 0 & -1/c^2 \\ 0 & -\rho c/2 & 0 & 1/2 \\ 0 & \rho c/2 & 0 & 1/2 \end{bmatrix}$$

and similarly for $[X_B]$ and $[X_B]^{-1}$.

References

[1]Lele, S. K., "Direct Numerical Simulation of Compressible Free Shear Flows," AIAA Paper 89-0374, Jan. 1989.

[2]Colonius, T., Lele, S. K., and Moin, P., "Scattering of Sound Waves by Compressible Vortex," AIAA Paper 91-0494, Jan. 1991.

[3]Mitchell, B. E., Lele, S. K., and Moin, P., "Direct Computation of Sound from a Compressible Co-Rotating Vortex Pair," *Journal of Fluid Mechanics*, Vol. 285, Feb. 1995, pp. 181–202.

[4]Tam, C. K., and Webb, J. C., "Dispersion–Relation–Preserving Schemes for Computational Aeroacoustics," *Journal of Computational Physics*, Vol. 107, No. 2, 1993, pp. 262–281.

[5]Watson, W. R., and Myers, M. K., "A Two-Step Method for Evolving Acoustic Systems to Steady-State," AIAA Paper 90-3946, Oct. 1990.

[6]Hixon, R., Shih, S.-H., and Mankbadi, R. R., "Valuation of Boundary Conditions for Computational Aeroacoustics," *AIAA Journal*, Vol. 33, No. 11, 1995, pp. 2006–2012.

[7]Lighthill, M. J., "On Sound Generated Aerodynamically, I. General Theory," *Proceedings of the Royal Society of London*, Series A, Vol. 211, 1952, pp. 564–587.

[8]Crow, S. C., "Aerodynamic Sound Emission as a Singular Perturbation Problem," *Studies in Applied Mathematics*, Vol. 49, March 1970, pp. 21–44.

[9]Powell, A., "Theory of Vortex Sound," *Journal of the Acoustical Society of America*, Vol. 36, Jan. 1964, pp. 177–195.

[10]Lyrintzis, A. S., "Review: The Use of Kirchhoff's Method in Computational Aeroacoustics," *Journal of Fluids Engineering*, Vol. 116, No. 4, 1994, pp. 665–676.

[11]Lyrintzis, A. S., and Mankbadi, R. R., "On the Prediction of the Far Field Jet Noise Using Kirchhoff's Formulation," AIAA Paper 95-0508, Jan. 1995.

[12]Freund, J. B., Lele, S. K., and Moin, P., "Calculation of Radiated Sound Field Using an Open Kirchhoff Surface," *AIAA Journal*, Vol. 34, No. 5, 1996, pp. 909–916.

[13]Hardin, J. C., and Pope, D. S., "An Acoustic/Viscous Splitting Technique for Computational Aeroacoustics," *Theoretical and Computational Fluid Dynamics*, Vol. 6, 1994, pp. 334–340.

[14]Hardin, J. C., and Pope, D. S., "Sound Generation by Flow over a Two-Dimensional Cavity," *AIAA Journal*, Vol. 33, No. 3, 1995, pp. 407–412.

[15]Lee, D. J., and Koo, S. O., "Numerical Study of Sound Generation Due to a Spinning Vortex Pair," *AIAA Journal*, Vol. 33, No. 1, 1995, pp. 20–26.

[16]Müller, E.-A., and Obermeier, F., "The Spinning Vortices as a Source of Sound," AGARD CP-22, 1967, pp. 22.1–22.8.

[17]Kim, J. W., and Lee, D. L., "Optimal Compact Finite Difference Schemes with Maximum Resolution," *AIAA Journal*, Vol. 34, No. 5, 1996, pp. 887–893.

[18]Courant, R., Isaacson, E., and Rees, M., "On the Solution of the Nonlinear Hyperbolic Differential Equations by Finite Differences," *Communications in Pure and Applied Mathematics*, Vol. 5, No. 2, 1952, pp. 243–255.

[19]Chakravarthy, S. R., Anderson, D. A., and Salas, M. D., "The Split Coefficient Matrix Method for Hyperbolic Systems of Gas Dynamic Equations," AIAA Paper 80-0286, Jan. 1980.

[20]Yates, J. E., "Application of the Bernoulli Enthalpy Concept to the Study of Vortex Noise and Jet Impigment Noise," NASA Rept. 2978, April 1978.

[21]Möhring, W., "On Vortex Sound at Low Mach Number," *Journal of Fluid Mechanics*, Vol. 85, 1978, pp. 685–691.

S. Glegg
Associate Editor